processes

MDPI

Article

Effects of Mineral Admixtures on the Evolution of Static Yield Stress of Different Composite Pastes

Yu Liu [1], Rui Jing [2] and Peiyu Yan [3,*]

[1] China Construction First Group Construction and Development Co., Ltd., Beijing 100102, China
[2] BCEG Advanced Construction Materials Co., Ltd., Beijing 100015, China
[3] Department of Civil Engineering, Tsinghua University, Beijing 100084, China
* Correspondence: yanpy@tsinghua.edu.cn

Abstract: The effects of different mineral admixtures on the evolution of static yield stress of common composite cementitious material paste and ultra-high-performance concrete (UHPC)-based paste were investigated. The results show that there are obvious differences in the role of mineral admixtures in the common paste and the UHPC-based paste. Adding mineral admixtures can change the initial static yield stress of the paste by affecting the particle size, particle shape and the charged particles. The addition of mineral admixtures with small particle size such as silica fume and ultrafine slag can increase the initial static yield stress of common paste but reduce that of UHPC-based paste. Adding mineral admixtures changes the evolution of static yield stress of the paste by affecting the particle spacing and the formation and growth rate of hydration products. In turn, the addition of ultrafine slag or silica fume increases the growth of the static yield stress of common paste. Adding slag, fly ash or fly ash microbeads successively reduces the static yield stress of common paste at the later stage. Affected by the content of PCE, the static yield stress of UHPC-based paste containing fly ash microbeads, slag, ultrafine slag and fly ash increases sequentially compared with the blank group at the later stage. The effect of silica fume with different dosages on the evolution of static yield stress of UHPC-based paste is significantly different.

Keywords: static yield stress; mineral admixture; paste; structural build-up; UHPC

Citation: Liu, Y.; Jing, R.; Yan, P. Effects of Mineral Admixtures on the Evolution of Static Yield Stress of Different Composite Pastes. *Processes* **2023**, *11*, 614. https://doi.org/10.3390/pr11020614

Academic Editor: Andrea Spagnoli

Received: 30 January 2023
Revised: 14 February 2023
Accepted: 16 February 2023
Published: 17 February 2023

1. Introduction

Three-dimensional printing concrete technology, also known as additive manufacturing of concrete, is a rapid prototyping technology based on 3D architectural models [1,2]. Due to the advantages of low labor cost, fast construction speed, no formwork and suitability for various construction sites, 3D printing concrete technology has been widely used [3,4]. Compared with traditional construction methods, 3D printing concrete technology can reduce construction waste by 30–60% and save more than 50% of labor cost and production time, while improving the digitization and intelligence of design [5].

In the process of 3D printing, on the one hand, the cementitious materials need good rheological properties to ensure that they can be effectively and continuously pumped and extruded through the nozzle. On the other hand, the cementitious materials need a suitable structural build-up rate after extrusion in order to obtain sufficient strength quickly to support themselves and the weight of the upper material layers [6]. The structural build-up rate of cementitious materials should not be high to avoid reducing the adhesion strength between the adjacent layers [7,8]. Therefore, it is crucial to control the structural build-up process of cementitious materials for the 3D printing process.

Cementitious materials, including concrete, mortar and paste, are all thixotropic materials [9,10]. Thixotropy is a reversible time-dependent phenomenon. The particles form a three-dimensional structure under the action of van der Waals attraction or electrostatic force at rest in the suspension, and the network is broken up to form individual floccule

during flow [11]. The flocculation and destruction of the structural network is influenced by shear history, material composition and shear strain rate [12,13]. In addition to the flocculation of particles at rest, other time-dependent changes of structure also occur in the fresh cementitious materials, resulting from the hydration of the cement, which are irreversible and result in the loss of their workability [14]. Therefore, the structural build-up of fresh cementitious materials at rest is a comprehensive development process associated with the combined action of both colloidal structuration formed by interaction between particles and chemical rigidification caused by cement hydration. Static yield stress testing, also known as stress growth testing, is a widely used test method to monitor the structural build-up of cementitious materials [15,16]. If cementitious materials are continuously sheared at a very low constant shear rate, the corresponding shear stress will show a peak or plateau value over time, which is the static yield stress. The structural build-up of the fresh cementitious materials can be characterized by the variation of static yield stress with time. N. Roussel [17] theoretically described the rheological properties of 3D printing concrete and demonstrated that its static yield stress is a key factor affecting the flow and continuous construction of 3D printing concrete. The constant shear rate used in the test varied between different studies. Mahaut et al. [18] used a constant shear rate of 0.01 s^{-1} to measure the development of the static yield stress of cement paste for 100 s per test. Perrot et al. [19] used a shear rate of 0.001 s^{-1}, which is one-tenth of the aforementioned shear rate, for 180 s to measure the static yield stress of cement paste and considered that the viscosity of the paste at this shear rate has no effect on the testing results. The results of Mahaut et al. [20] showed that although the flow of the paste could be ignored during the test, its structural network was still disturbed. Yuan et al. [21] studied the evolution of structural build-up of cement paste at different shear rates, such as 0.001 s^{-1}, 0.003 s^{-1}, 0.005 s^{-1}, 0.008s^{-1}, 0.01 s^{-1} and 0.02 s^{-1}, and compared the results with those of small amplitude oscillatory shear tests. Cheng et al. [22], Papo et al. [23], Coussot et al. [24], Roussel et al. [25] and Perrot et al. [26] respectively proposed the model to describe the process of structural build-up of cement paste.

A large amount of resources and energy are consumed in the production of Portland cement, accompanied by the emission of greenhouse gases such as carbon dioxide [27]. To reduce the usage of cement, achieve clean production of concrete and improve the mechanical properties and durability of concrete, different kinds of mineral admixtures have been widely utilized in practical engineering [28,29]. The utilization of these mineral admixtures affects the structural build-up process of fresh cementitious materials. Ahari et al. [30] studied the influence of different mineral admixtures on the process of the structural build-up of SCC and found that the addition of fly ash, silica fume and metakaolin could increase the rate of structural build-up. The opposite results were obtained by Khayat et al. [31]. Yuan et al. [32] measured the effects of 5% silica fume, 30% slag and 20% fly ash on the structural build-up of cement paste. The results showed that, at this content, the addition of silica fume can increase the growth rate of the static yield stress of the paste, while the slag and fly ash reduce it. Liu et al. [33] investigated the effects of fly ash, silica fume, cement and sand on the static yield stress of cementitious materials and determined the optimal composition of cementitious materials for 3D printing. The research of Chen et al. [34,35] showed that the addition of either bentonite or cellulose can increase the static yield stress of sulfoaluminate cement-based materials, thereby reducing the deformation of the printed layer. Kawashima et al. [36] added clay to the cement paste and found that the addition of clay enhanced the rate of structural build-up of the paste. Wang et al. [37] and Panda et al. [38] also found similar effects with nano-sized clay.

As mentioned above, the addition of mineral admixtures can affect the structural build-up of cementitious materials. New supplementary cementitious materials such as ultrafine slag and fly ash microbeads are gradually used to prepare concrete. The different mineral admixtures, such as slag and ultrafine slag, fly ash and fly ash microbeads, have similar chemical composition. However, there is still a lack of comparative studies on how they affect the process of the structural build-up of cementitious materials through their

respective physical and chemical interactions. Moreover, the application of UHPC in 3D printing has become increasingly popular, but the research on the effect of different mineral admixtures on the structural build-up of UHPC is still scarce. Simultaneously, there are few studies on the different effect of mineral admixtures on common composite cementitious material systems and UHPC in the process of structural build-up.

In this paper, the effects of different mineral admixtures on the time-dependent evolution of the static yield stress of common binder paste and UHPC-based paste were investigated. The influencing mechanism and the differences of different mineral admixtures in the two systems were analyzed to better understand and control the 3D printing process of cementitious materials.

2. Experimental

2.1. Materials

P·I 42.5 Portland cement conforming to Chinese National Standard GB 175–2007 (equivalent to European CEM I 42.5, EN197-1:2011 [39]) was utilized. Five mineral admixtures, including silica fume (SF), ground granulated blast furnace slag (GS), ultrafine slag (US), fly ash (FA) and fly ash microbeads (FC), were selected considering the application of mineral admixtures in practical engineering. The chemical compositions of the cement and mineral admixtures are shown in Table 1, and the densities are shown in Table 2. The particle size distribution of cementitious materials was measured using a laser particle size analyzer, as shown in Figures 1 and 2.

Table 1. Chemical compositions of cement and mineral admixtures *w*/%.

Material	SiO_2	Al_2O_3	Fe_2O_3	CaO	MgO	SO_3	Na_2O_{eq}	LOI
Cement	22.11	4.43	3.13	62.38	2.28	2.62	0.53	2.04
SF	96.36	0.33	0.05	0.58	0.34	1.05	0.86	2.11
GS	26.76	15.26	0.77	45.92	6.30	1.16	0.79	1.30
US	24.11	13.92	0.90	51.16	5.40	1.89	0.54	1.66
FA	45.52	34.39	7.34	6.45	0.70	0.60	1.22	5.08
FC	47.62	30.92	8.61	5.27	0.73	0.88	1.59	2.32

Note: $Na_2O_{eq} = Na_2O + 0.658K_2O$.

Table 2. Density of cement and mineral admixtures (g/cm^3).

Material	Cement	SF	GS	US	FA	FC
Density	3.15	2.24	2.89	2.89	2.34	2.47

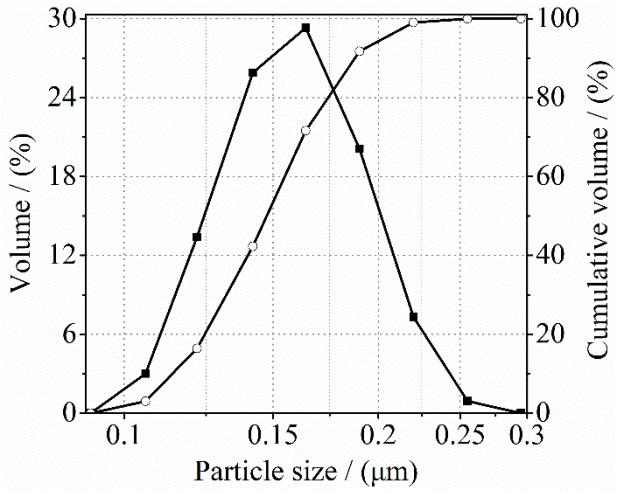

Figure 1. Particle size distributions of silica fume.

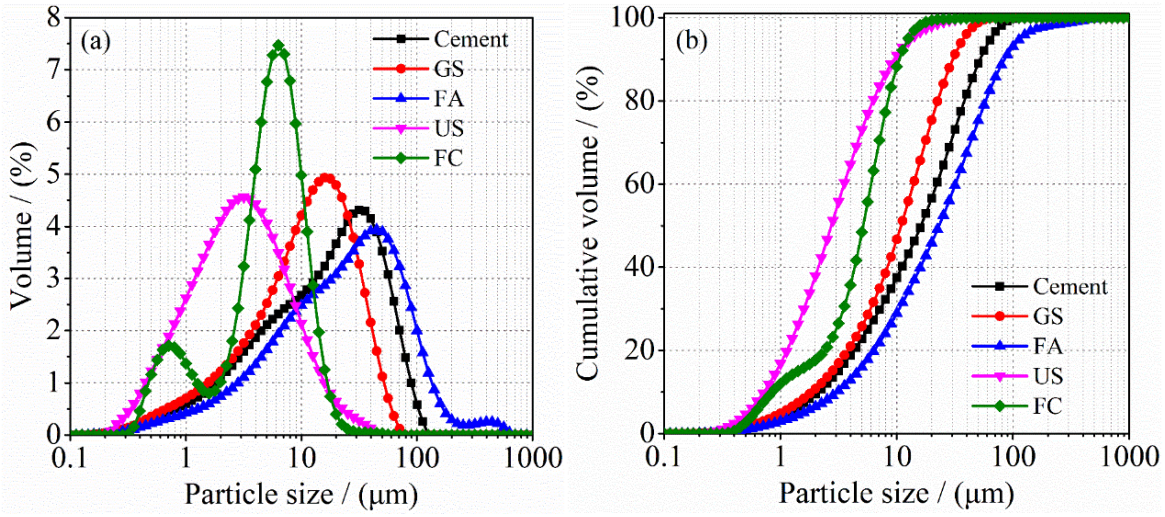

Figure 2. Particle size distributions of other cementitious materials: (**a**) differential curve, (**b**) cumulative curve.

Ghasemi et al. [40,41] proposed that the specific surface area of particles can be calculated according to the particle size distribution, as shown in Formula (1).

$$a_{poly} = \sum_{i=1}^{n} \frac{SA_i \omega_i}{V_i \rho_s} \quad (1)$$

where a_{poly} is the specific surface area, SA_i/V_i is the ratio of the surface area to the volume of the material in the particle size distribution, ω_i is the mass fraction in the particle size distribution and ρ_s is the density of the material. Based on the above calculation method and the particle size distribution of the particles (Figures 1 and 2), the calculated values of the specific surface area of the cementitious materials are obtained, as shown in Table 3. A commercially produced polycarboxylate superplasticizer (PCE) was used.

Table 3. Specific surface of cement and mineral admixtures (m^2/kg).

Material	Cement	SF	GS	US	FA	FC
Specific surface	367	17,195	446	1162	369	904

2.2. Mix Proportions

The different mix proportions of the investigated pastes are shown in Table 4. Cement was replaced by equal volumes of mineral admixtures with 10% and 20% content, respectively. The water-to-binder (W/B) ratios of pastes were set to 0.45 and 0.18, respectively. The paste with a W/B ratio of 0.45 was a common composite cementitious material system, and PCE was not added in order to determine the role of mineral admixtures in the process of the structural build-up of paste. The paste with a W/B ratio of 0.18 was set in order to explore the structural build-up of UHPC. PCE was added to the UHPC-based paste. The dosage of PCE was adjusted through the pre-experiment so that the fluidity of pastes remained almost 210 mm, except for CSF20-0.18 and CFA20-0.18, which were 190 mm.

Table 4. Mix proportions of pastes.

Samples	Cement (*v*/%)	SF (*v*/%)	GS (*v*/%)	US (*v*/%)	FA (*v*/%)	FC (*v*/%)	PCE (*w*/%)	W/B Ratio
REF-0.45	100	-	-	-	-	-	-	0.45
CSF10/20-0.45	90/80	10/20	-	-	-	-	-	0.45
CGS10/20-0.45	90/80	-	10/20	-	-	-	-	0.45
CUS10/20-0.45	90/80	-	-	10/20	-	-	-	0.45
CFA10/20-0.45	90/80	-	-	-	10/20	-	-	0.45
CFC10/20-0.45	90/80	-	-	-	-	10/20	-	0.45
REF-0.18	100	-	-	-	-	-	0.8	0.18
CSF10/20-0.18	90/80	10/20	-	-	-	-	0.74/1.1	0.18
CGS10/20-0.18	90/80	-	10/20	-	-	-	0.62/0.53	0.18
CUS10/20-0.18	90/80	-	-	10/20	-	-	0.55/0.45	0.18
CFA10/20-0.18	90/80	-	-	-	10/20	-	0.85/0.95	0.18
CFC10/20-0.18	90/80	-	-	-	-	10/20	0.6/0.49	0.18

2.3. Test Methods

2.3.1. Test for Structural Build-Up of Paste

The structural build-up of fresh paste was measured using an Anton Paar MCR302 coaxial-cylinder rheometer. The surface of the rotor and outer cylinder is serrated to prevent the paste from slipping during testing. The diameters of the rotor and outer cylinder are 26.660 mm and 28.911 mm respectively, and the shear gap size is 1.126mm. Before the test, all the components of the mixture were placed in an environment of 25 °C. The temperature control system of the rheometer was also set at 25 °C during the measurement. The test was repeated three times, and the average value of the three experiments results was taken as the final result.

The materials, weighted according to the mix proportions, were fully mixed for 8 min. In order to achieve the same initial state of pastes and eliminate the influence of the mixing history, pastes were pre-sheared before testing to ensure the good repeatability [12]. The effect of pre-shearing can be enhanced by applying large amplitude oscillatory shear [42], which makes paste close to a liquid. The pre-shear process consisted of shearing pastes for 90 s at a shear rate of 200 s^{-1} followed by 10 s of large amplitude oscillatory shear at a shear strain of 6% and an angular frequency of 100 rad/s. It was found that the storage modulus of pastes was almost 0 after pre-shearing, indicating an initial state of pastes similar to that of liquid. The static yield stress of pastes was determined 15 min after the contact of cementitious materials with water.

The shear rate value applied during the measurement is important. The structural network of pastes is strengthened by the continuous hydration of the binder. If the shear rate applied is too low, the time to reach the strain value required for paste to flow is too long, and the resulting static yield stress will no longer be the resulting value at the desired moment. When the shear rate used is too high, the damage to the structural network of paste will be more serious. For the two composite cementitious material systems in this study, different shear rates were determined through the pre-experiment. For common pastes, the initial static yield stress of pastes was measured with a shear rate of 0.1 s^{-1} immediately after pre-shearing, and the test time was 60 s. After that, the static yield stress of pastes was measured every 10 min with a shear rate of 0.005 s^{-1}, and each test time was 15 s. The total test duration was 2 h. The higher shear rate was utilized to study the initial static yield stress because the time required for shear stress to peak was too long at low shear rates. The testing procedure for the UHPC-based pastes is similar to the common pastes. The only difference is the initial shear rate of 0.01 s^{-1}.

2.3.2. Water Film Thickness

The packing density of the cementitious materials, the surface area of the solid particles and the water content all affect the rheological properties of the fresh paste [43]. The

combined effect of these factors can be characterized by the water film thickness on particles. Kwan et al. [44] described that a part of the water in the cementitious materials paste was used to fill the voids among particles, and the remaining water would wrap around the surface of particles to form a water film. The wet packing density of two composite systems was determined using the test method proposed by Kwan et al. [45,46], respectively. The testing process is described below:

(1) Different W/B ratios at which the wet packing test was to be carried out were set. The required quantities of materials, water and PCE were weighed.
(2) All powder materials were then premixed for 2 min.
(3) Next, all the water, half of the cementitious materials and PCE were added to a mixing bowl and stirred for 2 min.
(4) The remaining cementitious materials and PCE were divided into four equal parts, then one part of cementitious material and PCE was added each time and stirred for 3 min.
(5) After mixing, the paste was poured into the prepared volumetric cylinder. The surface of the cylinder was scraped, and the mass of the paste was weighed.
(6) The above steps were repeated under different W/B ratios, and then the following expressions were applied to calculate the solid concentration and voids ratio of the system based on the measured mass of paste, until the maximum solid concentration and minimum voids ratio were found.

$$V_c = \frac{M}{\rho_w u_w + \rho_\alpha R_\alpha + \rho_\beta R_\beta + \rho_\gamma R_\gamma} \quad (2)$$

$$\varnothing = V_c / V \quad (3)$$

$$\vartheta = (V - V_c)/V_c \quad (4)$$

where M and V are the mass and volume of paste in the volumetric cylinder, respectively; ρ_w is the density of water; u_w is the volume ratio of water to cementitious materials; ρ_α, ρ_β and ρ_γ are the densities of different cementitious materials, respectively; R_α, R_β and R_γ are the volume fraction of different cementitious materials; V_c is the solid volume of cementitious materials; $\varnothing$ is the solid concentration of paste and its maximum value is the wet packing density and ϑ is the voids ratio of paste.

The water film thickness of paste can be calculated with the test results and the following expression.

$$u'_w = u_w - \vartheta \quad (5)$$

$$A_M = A_\alpha \times R_\alpha + A_\beta \times R_\beta \quad (6)$$

$$WFT = \frac{u'_w}{A_M} \quad (7)$$

where u'_w is the proportion of remaining water (the ratio of the volume of remaining water to the volume of solid), A_M is the specific surface area (surface area per unit volume of solid), A_α and A_β are the specific surface areas of cement and mineral admixtures, respectively, and WFT is the water film thickness. The test was repeated three times, and the average value of the three experiments results was taken as the final result.

3. Results and Discussion

3.1. Common Pastes

3.1.1. Initial Static Yield Stress

The change of shear stress of common pastes with time at the initial time is shown in Figure 3. After pre-shearing, the paste is in a viscous state with fully dispersed particles at the initial moment. In the case of continuous shear of the paste, the shear stress peak of most pastes appears between 30 s and 40 s. This is the initial static yield stress (Figure 4).

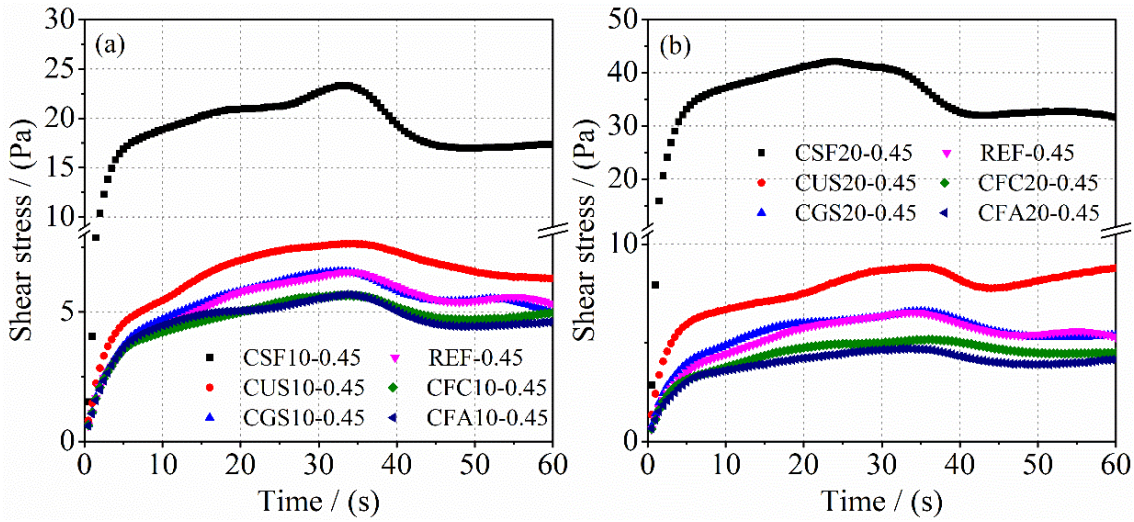

Figure 3. The change of shear stress of common pastes with time at the initial stage: (**a**) 10%, (**b**) 20%.

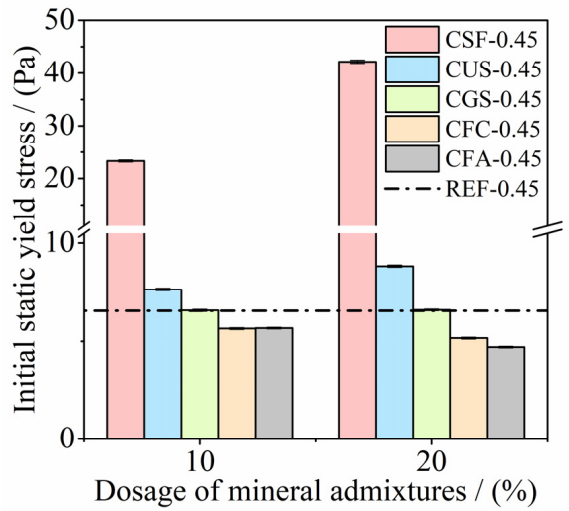

Figure 4. The initial static yield stress of common pastes.

The static yield stress of blank common paste with W/B of 0.45 is 6.55 Pa when the particles are completely dispersed. The addition of silica fume significantly increases the initial static yield stress of pastes. The initial static yield stress of CSF10-0.45 and CSF20-0.45 systems was 3.56 times and 6.44 times that of the blank group, respectively. The addition of ultrafine slag also increases the initial static yield stress of the paste, but the effect is not as significant as that of silica fume. The initial static yield stress of pastes with different content of slag is almost the same as that of the blank group. However, the initial static yield stress of pastes decreases with the increasing dosage of fly ash or fly ash microbeads. The value is the minimum when fly ash is added.

3.1.2. The Evolution of Static Yield Stress

When the shear rate is 0.005 s^{-1}, the variation of shear stress of common pastes with time is shown in Figure 5. It can be seen that the time for the shear stress to peak is short. According to Figure 5, the effect of mineral admixtures with different dosages on the evolution of the static yield stress of pastes over time can be obtained, as shown in Figure 6. When silica fume or ultrafine slag is added, the static yield stress of the paste is enhanced with the increase of mineral admixture content at any test time. Among them, the increase of the static yield stress of the paste with silica fume is the most obvious. When fly ash microbeads are added, the static yield stress of the paste mixed with 10% of fly

ash microbeads is the largest within about 20 min after the start of the test, and then the static yield stress of the paste with fly ash microbeads is gradually smaller than that of the blank group. However, within about 50 min after the start of the test, the difference among the static yield stress values of different pastes is small. The static yield stress of the paste decreases with the increase of fly ash content at the same test moment. Similarly, the difference between the static yield stress values of different pastes is small at the initial stage of the test, but the variation range increases with the prolongation of test time. The static yield stress of the paste containing slag decreases slightly with the increase of slag content, but the change is not significant.

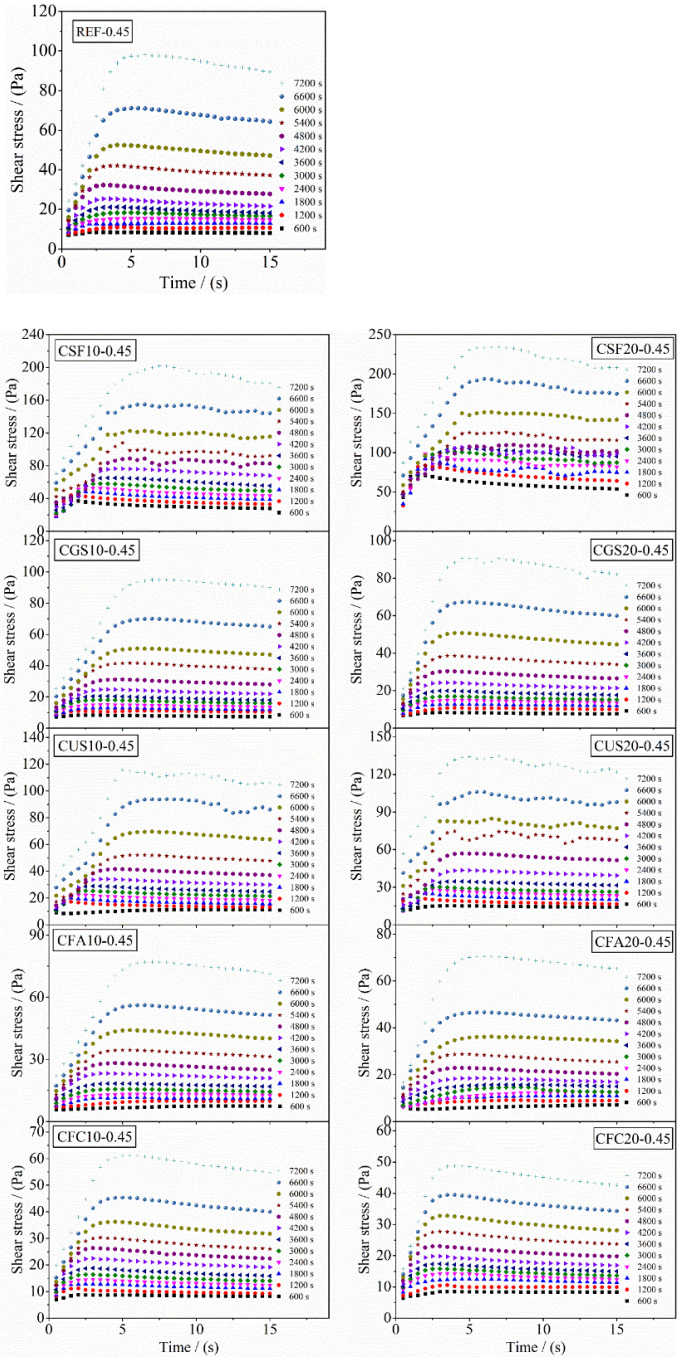

Figure 5. The change of shear stress of common pastes with time at each test stage.

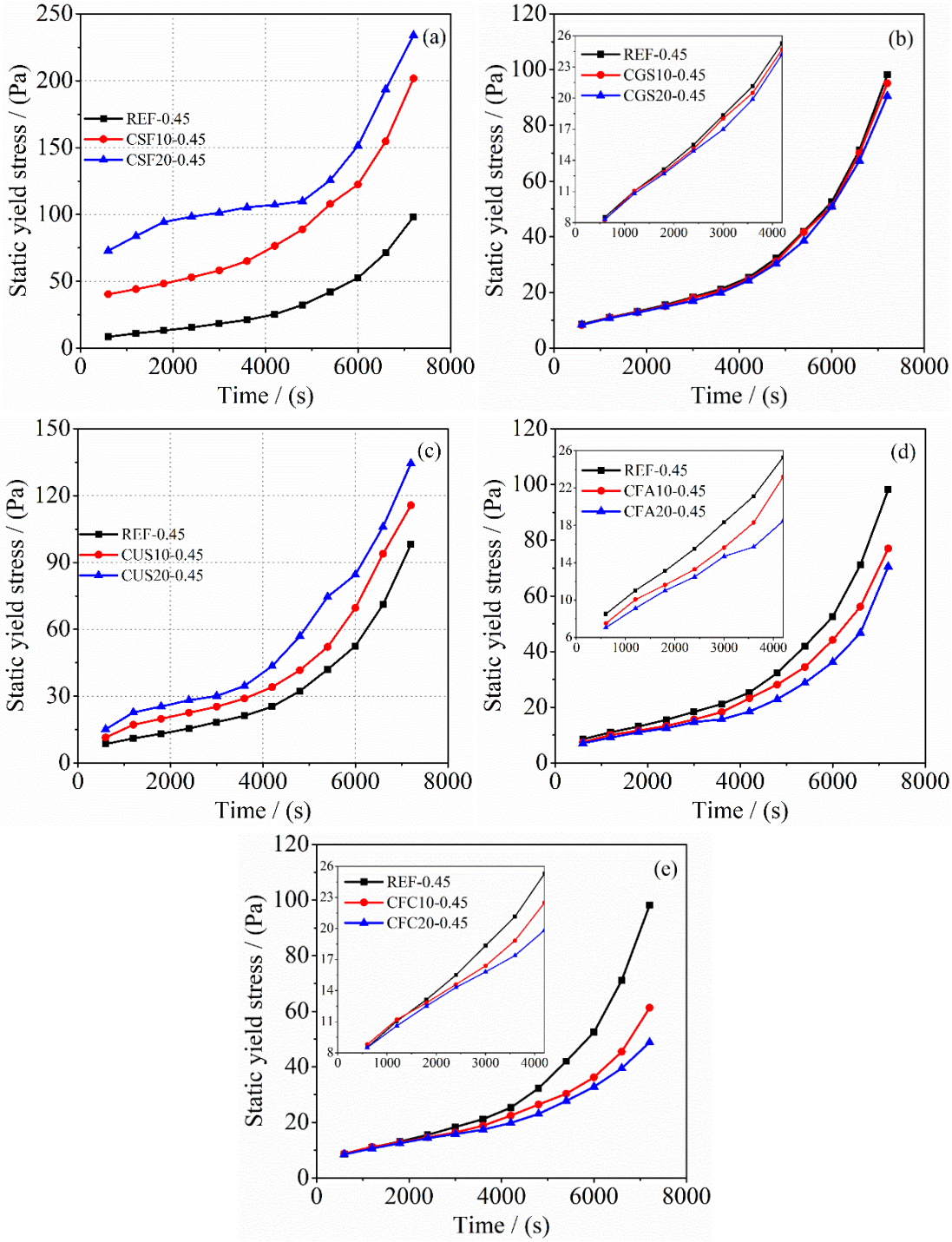

Figure 6. Effect of mineral admixtures on the evolution of static yield stress of common pastes: (**a**) CSF-0.45, (**b**) CGS-0.45, (**c**) CUS-0.45, (**d**) CFA-0.45, (**e**) CFC-0.45.

According to Figure 5, the influence of different mineral admixtures with the same dosage on the development of the static yield stress of pastes over time can be obtained, as shown in Figure 7. The ability of silica fume to increase the static yield stress of paste is the strongest, followed by ultrafine slag. The static yield stress of paste mixed with slag or fly ash is lower than that of the blank group at any test moment, among which the static yield stress of paste mixed with slag is higher. The static yield stress of the paste containing a small amount of fly ash microbeads is slightly higher than that of the blank group at the initial stage, but over time it is gradually lower than that of the blank group, the paste

with slag and the paste with fly ash. The static yield stress of the paste containing fly ash microbeads is the smallest at the later stage.

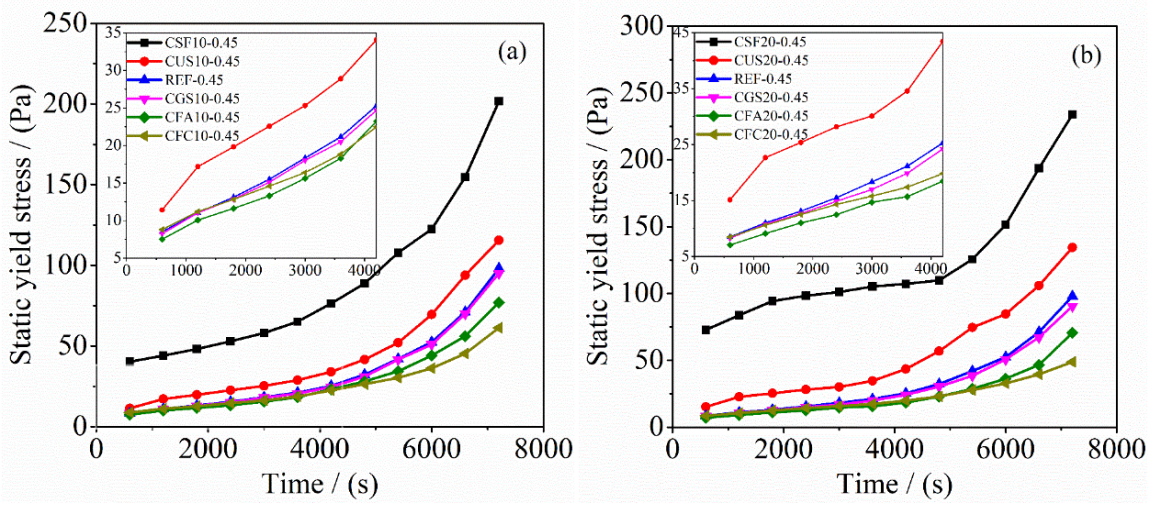

Figure 7. Effect of different mineral admixtures on the evolution of static yield stress of common pastes: (**a**) containing 10% of mineral admixture, (**b**) containing 20% of mineral admixture.

The wet packing density of each paste was tested, and its water film thickness was then calculated, as shown in Figure 8. The average distance between particles can be characterized by the water film thickness.

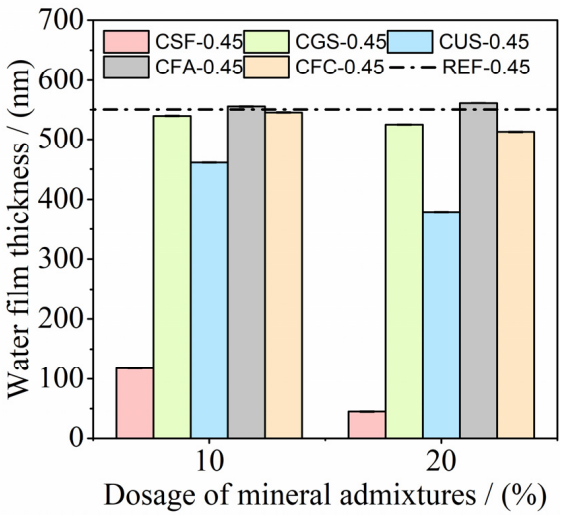

Figure 8. The water film thickness of common pastes.

3.2. UHPC-Based System

3.2.1. Initial Static Yield Stress

The evolution of the shear stress of UHPC-based pastes over time obtained at the initial moment is shown in Figure 9. The paste is in the viscous state, with fully dispersed particles. The shear stress of pastes does not reach a peak value but forms a stable plateau value at 120 s. This value is taken as the static yield stress of UHPC-based pastes, as shown in Figure 10. The test time has not been further extended to obtain the decreasing stage of shear stress. When the test time is too long, the static yield stress obtained will no longer be the result of the expected time due to the change of paste structure. Overall, the initial static yield stress of UHPC-based pastes is lower than that of common pastes. The initial static yield stress of UHPC-based paste can be effectively reduced by adding 10% silica fume.

With the increase of silica fume dosage, the initial static yield stress of pastes increases greatly. The initial static yield stress of UHPC-based paste mixed with 20% silica fume is about three times that of the blank group. The addition of fly ash also increases the initial static yield stress of the paste, which is higher than that of other samples. When slag, fly ash microbeads and ultrafine slag are added, the initial static yield stress of UHPC-based pastes gradually decreased.

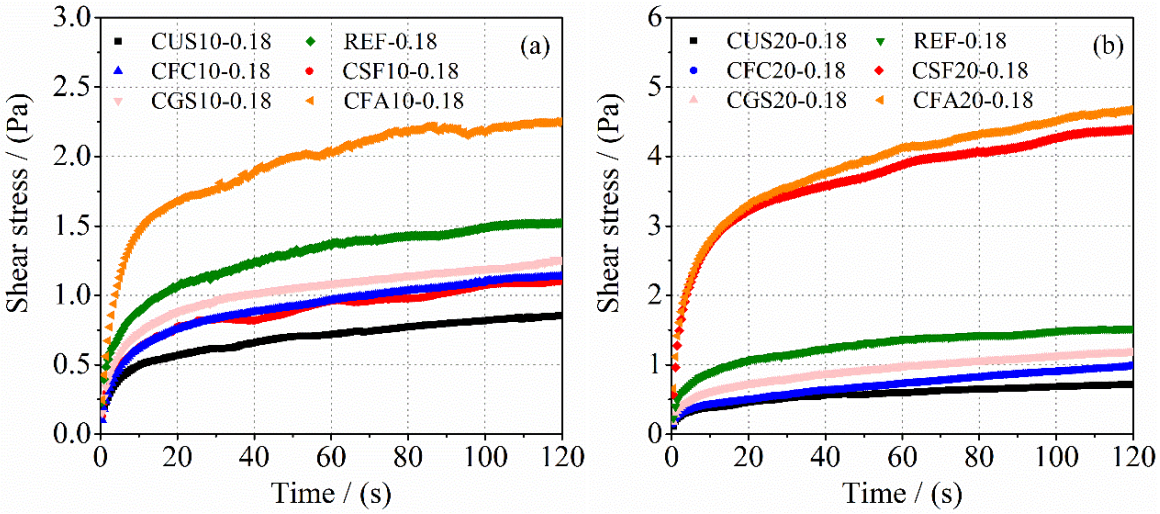

Figure 9. The change of the shear stress of UHPC-based pastes with time at the initial stage: (**a**) containing 10% of mineral admixture, (**b**) containing 20% of mineral admixture.

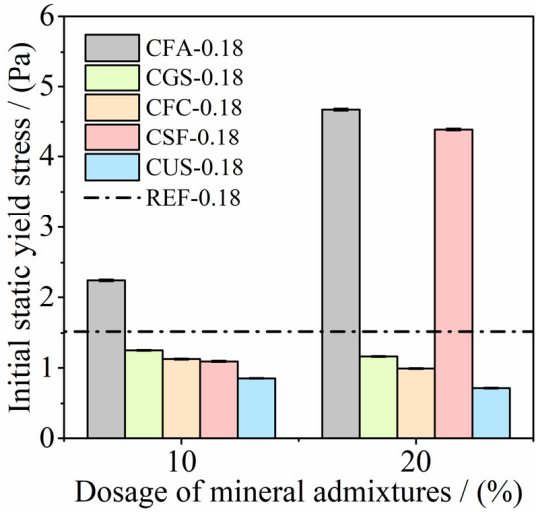

Figure 10. The initial static yield stress of UHPC-based pastes.

3.2.2. The Evolution of Static Yield Stress

The variation of shear stress of UHPC-based pastes with time at each test stage is shown in Figure 11. It can be seen that, at some test stages, it takes a long time for the shear stress to reach the peak value.

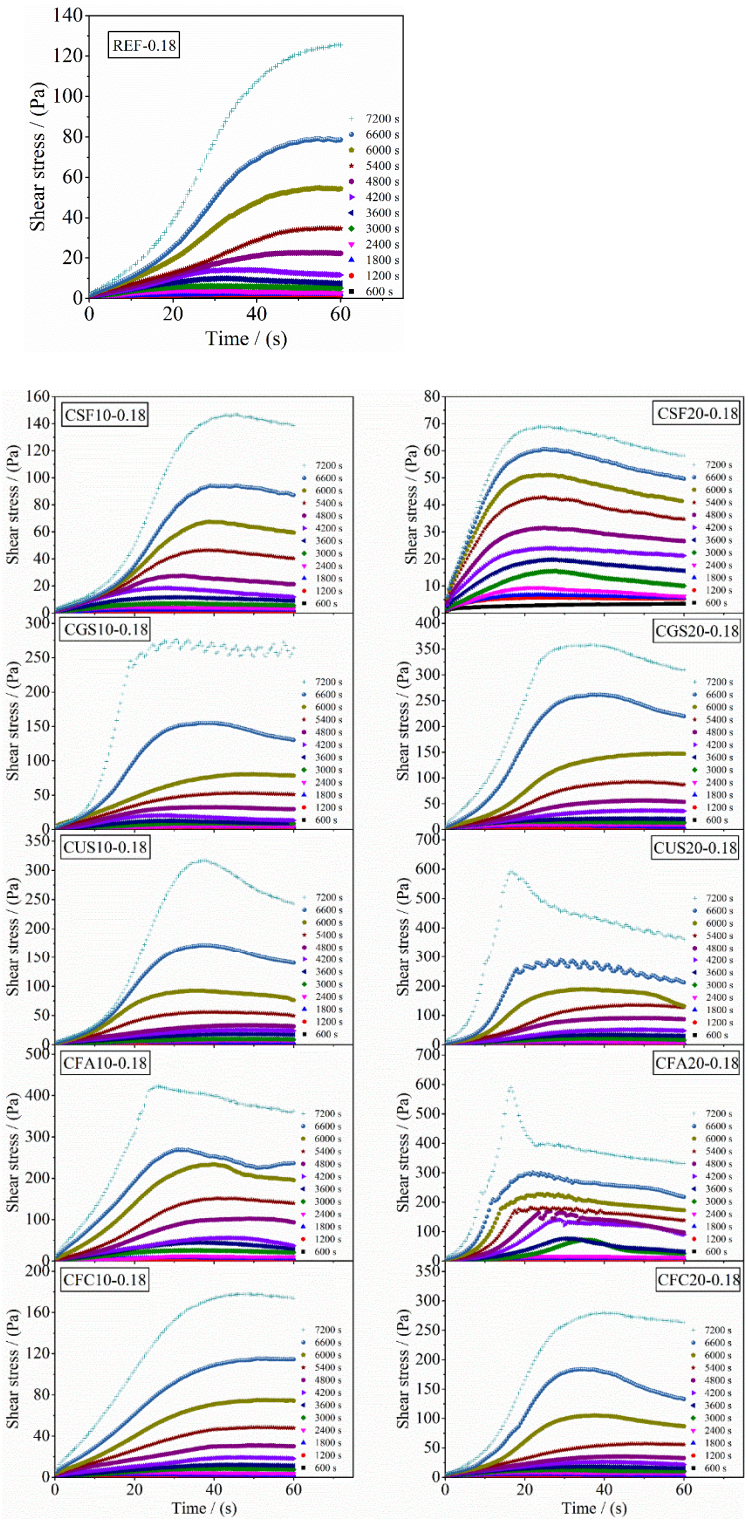

Figure 11. The change of shear stress of UHPC-based pastes with time at each test stage.

The role of mineral admixtures in the process of the structural build-up of UHPC-based paste is significantly different from that of common paste. According to Figure 11, the influence of mineral admixtures with different dosages on the evolution of static yield stress of UHPC-based paste is obtained, as shown in Figure 12. It can be seen that with the addition of ultrafine slag or fly ash microbeads, the static yield stress of the paste decreases slightly with the increase of mineral admixture content within the initial 20 min, and is lower than that of other samples. With the prolongation of time, the static yield stress of

both samples is enhanced with the increase of mineral admixture content. The static yield stress of pastes increases with the increase of slag or fly ash content. The static yield stress of pastes also increases with the increase of silica fume content in the first half of the test, but then the static yield stress of CSF20-0.18 is gradually lower than that of CSF10-0.18 and the blank group. In the first half of the measurement, the static yield stress of pastes is little affected by the change of mineral admixture content. With the continuous progress of cement hydration, the influence of mineral admixtures on the static yield stress of pastes is gradually enhanced.

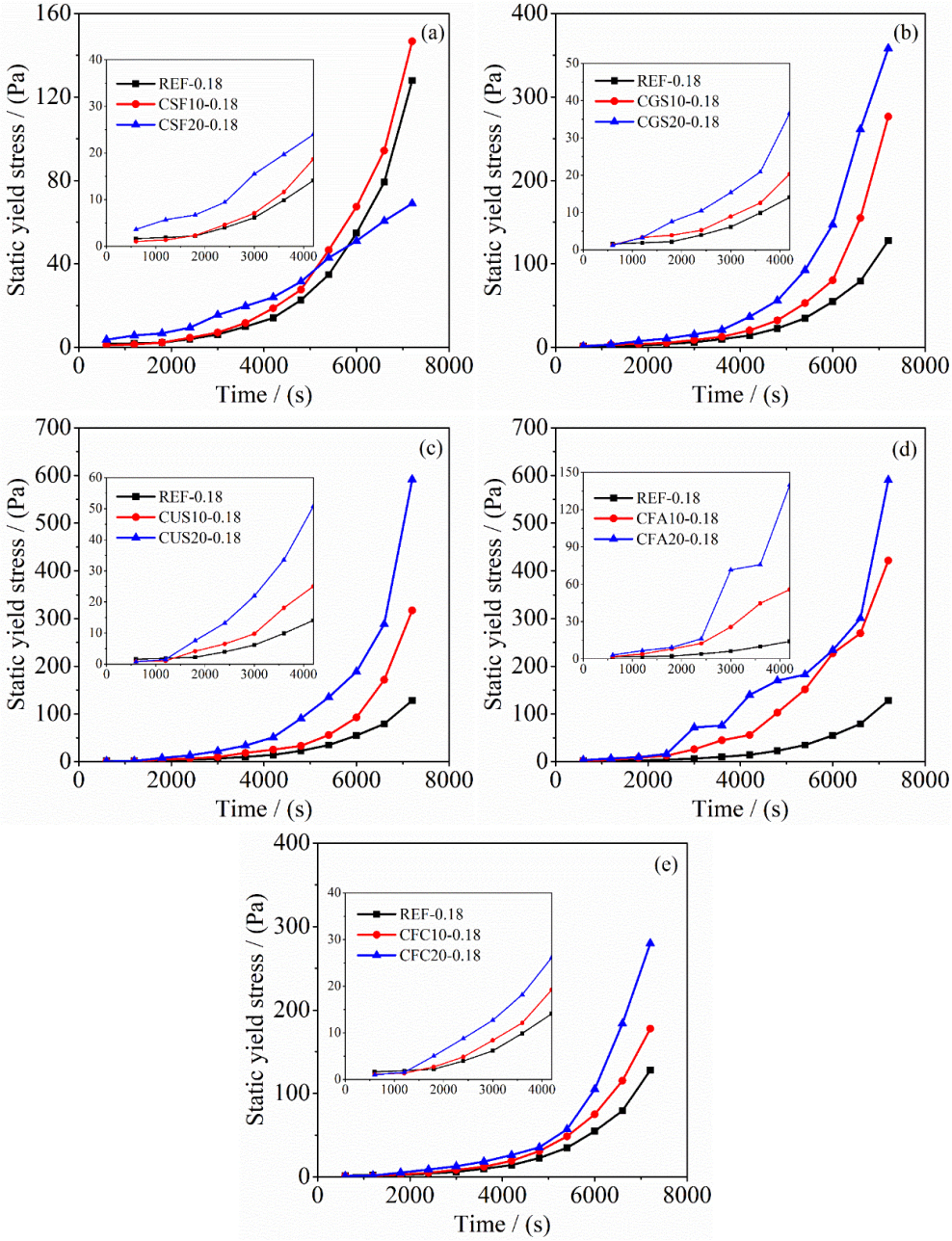

Figure 12. Effect of mineral admixtures on the evolution of the static yield stress of UHPC-based pastes: (**a**) CSF-0.18, (**b**) CGS-0.18, (**c**) CUS-0.18, (**d**) CFA-0.18, (**e**) CFC-0.18.

Figure 13 shows the effects of different mineral admixtures with the same dosage on the development of the static yield stress of UHPC-based pastes over time. When the content of mineral admixture is 10%, the static yield stress of pastes containing fly ash is

maximum at any test time. During the first 20 min of the test process, the addition of fly ash or slag increases the static yield stress. The addition of ultrafine slag, fly ash microbeads or silica fume reduces the static yield stress of pastes, and then the static yield stress of the three is gradually higher than that of the blank group. At the later test stage, the static yield stress of the pastes containing silica fume, fly ash microbeads, slag, ultrafine slag or fly ash increases successively compared with the blank group. In fact, in the first 80 min of the test, except for the paste containing fly ash, there is no significant difference in the static yield stress of pastes. When the content of mineral admixture is 20%, the static yield stress of the paste containing fly ash is the highest. In the first 20 min of the test process, the static yield stress of the paste with silica fume is close to that with fly ash and higher than that of the other systems, but gradually lower than that of other systems, along with the development of cement hydration. At the later stage of the test, the static yield stress of the paste containing silica fume; the blank group and the paste containing fly ash microbeads, slag, ultrafine slag and fly ash increases sequentially.

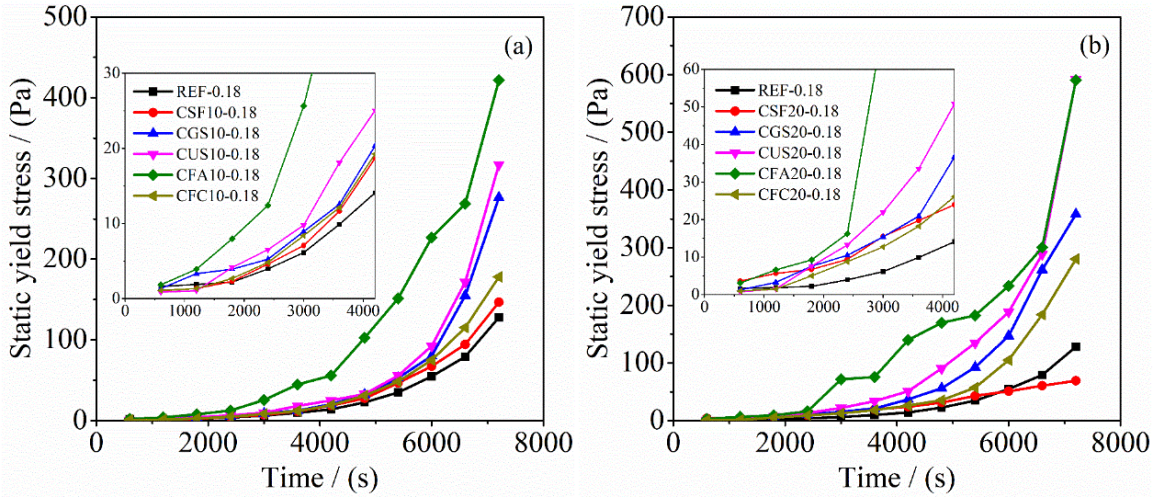

Figure 13. Effect of different mineral admixtures on the evolution of static yield stress of UHPC-based pastes: (**a**) containing 10% of mineral admixture, (**b**) containing 20% of mineral admixture.

The water film thickness of UHPC-based pastes is shown in Figure 14.

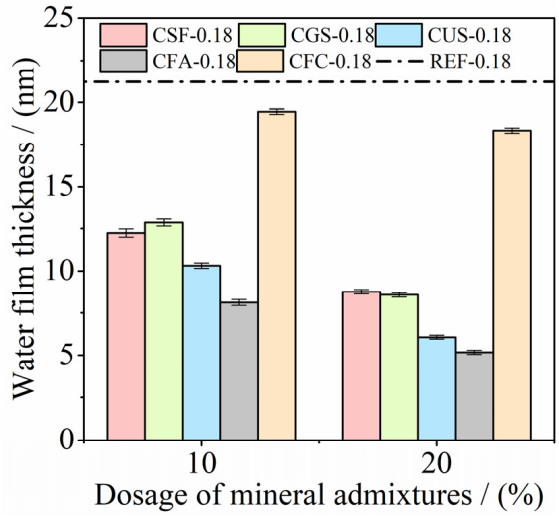

Figure 14. The water film thickness of UHPC-based pastes.

3.3. Discussion

3.3.1. Influence Mechanism of Mineral Admixture on Initial Static Yield Stress of Paste

The static yield stress is the force that the paste needs to overcome when it starts to flow from a static state. The whole process includes the destruction of flocculation and bridging among particles and the movement of particles. At the beginning of the test, the paste structure is in a completely dispersed state, so the static yield stress is the force that pushes particles to move. However, due to the low shear rate and small shear deformation, the past cannot start to flow immediately. Meanwhile, the mineral phases of cement such as C_3A and C_3S have dissolved, and there are Ca^{2+}, OH^-, $SiO_3{}^{2-}$, $SO_4{}^{2-}$ and Al^{3+} in the liquid phase. Particles of different mineral phases may have opposite electrical charges on their surfaces. Particles flocculate rapidly under the influence of various interaction forces such as electrostatic force, van der Waals attraction and Brownian force. In addition, needle-like AFt generates by hydration of C_3A within a few minutes after it encounters water and bridges solid particles. Under these two conditions, a structural network is formed in the paste. Thus, the initial static yield stress is the combination of the force that pushes the particles and the force that destroys the formed structural network.

Adding silica fume or ultrafine slag increases the number of small-sized particles in pastes. The Brownian motion of small particles is strong, which speeds up the collision frequency of particles and brings them close to each other. Therefore, they can be trapped by the attractive field of surrounding particles. The addition of small particles can also promote the dissolution of cement particles during mixing. The number of charged particles and rapidly generated AFt in paste increases to result in an enhancement of the flocculation capacity of paste. Therefore, adding silica fume or ultrafine slag can increase the rate of the structural build-up of paste, thereby increasing its initial static yield stress. Silica fume has the smallest particle size, and the effect is the most significant. The particle shape of slag is similar to that of cement, but its particle size is slightly smaller than that of cement, which slightly increases the number of small particles in the paste. However, due to the reduction of cement content in paste, the number of charged particles and AFt decreases, resulting in the initial static yield stress of the paste remaining unchanged. The addition of fly ash microbeads also increases the number of small particles in paste, but the smooth surface of fly ash microbeads reduces the flocculation capacity of particles and the friction among particles. When the fly ash is added, the average particle size increases and the friction force among the particles is reduced at the same time. The cement content in paste also decreases. The initial static yield stress of paste containing fly ash decreases.

After a large amount of PCE was added, the steric hindrance and electrostatic action of PCE weaken the flocculating and bridging ability of particles. Therefore, the initial static yield stress of UHPC-based pastes is low. In addition, the high content of solid particles in UHPC-based pastes makes for a difficult movement of particles. Small particles such as ultrafine slag and fly ash microbeads disperse among large particles, which enhances a rolling among particles. Within a certain size range, the smaller the particles are, the more obvious the rolling effect is. The effect of slag, fly ash microbeads and ultrafine slag enhances successively. Because the PCE content in pastes also decreases in turn, the initial static yield stress of the three is not significantly different. The low dosage of silica fume can also enhance the relative motion among particles, thereby reduce the initial static yield stress of pastes. The flocculation tendency of particles in paste is greatly enhanced with high silica fume content; then, the initial static yield stress of pastes increases. The carbon content of fly ash is high, meaning that it can adsorb a significant amount of PCE and enhance the tendency of flocculation among binder particles. The average particle size of fly ash is large, which will hinder the relative motion of particles and strengthen the friction and collision among particles in the paste with high solid content. Thus, the initial static yield stress of the paste with fly ash increases. Meanwhile, it can be seen that the effect of ultrafine slag, fly ash and a small amount of silica fume on the initial static yield stress of common paste and UHPC-based paste is significantly different.

3.3.2. Influence Mechanism of Mineral Admixture on the Evolution of Static Yield Stress of Paste

The common paste in the state of complete dispersion of particles will form a stable percolation network with a certain strength through the interaction force among particles after tens to hundreds of seconds. Subsequently, the percolation network of pastes is gradually strengthened under the action of binder hydration. The study of Jansen et al. [47] showed that the main hydration reaction of fresh cement paste during the induction period was the generation of AFt, and the change of the rheological properties of pastes in this period had a good correlation with the increase in the amount of AFt. The hydration rate of fresh cement paste was mainly dominated by the precipitation rate of C-S-H during the acceleration period [48]. Therefore, with the progress of cement hydration, different hydration products grow and bridge particles, resulting in a gradual enhancement of the percolation network of pastes, which in turn leads to an increase in their static yield stress. The main factors affecting the enhancement of the percolation network of pastes are the distance between particles and the generation and growth rate of hydration products.

The average distance between particles of the paste mixed with silica fume or ultrafine slag is significantly reduced, which allows the hydration products to precipitate easily and bridge particles. Moreover, the mineral admixture particles with small particle size can accelerate the dissolution of cement and nucleation of hydrates during the mixing and hydrating process of pastes, thus increasing the generation and growth rate of hydration products. Therefore, the static yield stress of paste increases. When slag is added, the average distance between particles slightly reduces. However, as the cement content in the paste decreases, the production of hydration products reduces, so the static yield stress of the paste decreases slightly compared with that of the blank group. When adding fly ash microbeads, the distance between particles also slightly reduces. Compared with slag, the number of small particles of fly ash microbeads significantly increases, which results in an accelerated dissolution of cement. Therefore, at the initial stage of the test, the static yield stress of the paste with fly ash microbeads is higher than that of the paste with slag. However, its static yield stress is gradually lower than that of other groups because fly ash microbeads have an obvious postponing effect on cement hydration, thus reducing the production of hydration products. When fly ash is added, the average distance between particles in the paste increases slightly, and the average particle size of fly ash is larger than that of cement. Fly ash also has a postponing effect on cement hydration. Therefore, at the initial stage of the test, the static yield stress of the paste mixed with fly ash is the minimum. However, the static yield stress of paste with fly ash microbeads is smaller at the same dosage at the later test period.

Compared with the common pastes, the main differences of UHPC-based pastes in composition are the high content of solid particles and the addition of PCE (Table 4). By changing the packing distribution of particles and the hydration reaction rate of the binder, the structural build-up of pastes and their time-dependent development of the static yield stress are influenced. First, PCE with anionic charges adsorbs on the surface of dissolved cement particles. The steric hindrance and electrostatic repulsion of PCE make it difficult for binder particles to approach each other. Binder particles cannot flocculate and form a percolation network quickly due to the interaction forces such as van der Waals attraction and electrostatic attraction. The particles are in a state of loose packing in pastes. At the same time, PCE can hinder the early hydration of the binder and reduce the formation and growth rate of hydration products, thus affecting the speed of particle bridging. Therefore, the static yield stress of UHPC-based pastes grows slowly at the early stage. Moreover, except for individual groups such as CUS20-0.18, most systems are still in the induction period of hydration when the test time reaches 2.25 h.

When the dosage of silica fume is 10%, the mutual movement of binder particles under shear stress is enhanced by the tiny silica fume particles, thereby reducing the static yield stress of pastes in the first 20 min. The average particle distance and PCE content of CSF10-0.18 are lower than those of the blank group, which enhances its rate of structural

build-up. The static yield stress of pastes thus gradually increases compared with the blank group. However, the content of PCE in CSF10-0.18 is still higher than that of other systems. Meanwhile, the addition of silica fume retards the cement hydration at the early stage. The formation and growth rate of hydration products are low, resulting in the static yield stress of the paste being lower than that of other systems at the same time. When 20% silica fume is added, the percolation network forms in the paste at the early stage, and its static yield stress is higher than that of other pastes. However, the PCE content of CSF20-0.18 is much higher than that of other pastes (Table 4), and the effect of silica fume on inhibiting binder hydration is also more obvious, so the static yield stress of the paste is the lowest at the later stage.

When fly ash microbeads are added, the movement and rolling of binder particles can also be enhanced, and the static yield stress of the paste decreases within the first 20 min. The addition of fly ash microbeads can retard binder hydration and reduce the formation and growth rate of hydration products. The cement content of the paste also decreases, and the average distance between particles is higher than that of other pastes. However, the PCE content of CFC10-0.8 and CFC20-0.18 decreases significantly compared with the blank group (Table 4). Under the comprehensive influence, the static yield stress of the CFC system is higher than that of the blank group and the CSF system but lower than that of other systems, and it increases with the growth of fly ash microbeads content.

The structural build-up rate of the paste containing fly ash is significantly enhanced. Although the addition of fly ash retards the hydration of cement, carbon in fly ash can adsorb a significant amount of PCE in the paste, which reduces the adsorption amount of PCE on the surface of cement particles. The dispersing effect of PCE on cement particles and the effect of retarding cement hydration are weakened. Simultaneously, the average particle distance of the CFA system is the smallest, which greatly increases the static yield stress of the paste.

When slag or ultrafine slag is added, the PCE content of the paste decreases gradually with the increase of mineral admixture content. The addition of mineral admixture does not retard the hydration of cement, so the static yield stress of two systems is only lower than that of the CFA system. The CUS system has higher static yield stress because the content of PCE (Table 4) and the average distance of particles in the paste (Figure 14) are smaller than those of the CGS system. In addition, similar to the addition of fly ash microbeads or low content of silica fume, the addition of ultrafine slag can reduce the static yield stress of the paste at the initial stage of the test.

4. Conclusions

In this paper, the influence of different mineral admixtures on the evolution of static yield stress of fresh paste over time is investigated. It is found that there are obvious differences in the role of mineral admixtures in common pastes and UHPC-based pastes. The main conclusions are as follows:

(1) The initial static yield stress of pastes is the combination of the force that pushes the particles to move and the force that destroys the structural network that rapidly forms during the test (within tens of seconds). For the common pastes, the strong Brownian motion of small particles and its effect of promoting the dissolution of cement particles can increase the initial static yield stress of pastes. The addition of ultrafine slag or silica fume increases the initial static yield stress of pastes in turn, while the addition of fly ash or fly ash microbeads successively reduces the initial static yield stress of the paste. Adding slag has no effect on the initial static yield stress of the paste.

(2) For UHPC-based pastes with similar fluidity, the addition of small particles can promote the relative movement among particles under the shear force, thus reducing the initial static yield stress of pastes. The initial static yield stress of pastes can be effectively decreased by adding 10% of silica fume. With the increase of the silica fume content, the initial static yield stress of paste increases greatly. Addition of fly ash also increases the static yield stress of paste, which is higher than that of other

systems. When slag, fly ash microbeads or ultrafine slag are added, the static yield stress of pastes gradually decreases.

(3) The main factors affecting the evolution of static yield stress of pastes are the particle distance and the formation and growth rate of hydration products. For common pastes, at any test moment, silica fume has the strongest ability to increase the static yield stress of pastes, followed by ultrafine slag. The static yield stress of the paste containing slag or fly ash is successively lower than that of the blank group. The static yield stress of the paste with small dosage of fly ash microbeads is slightly higher than that of the blank group at the early stage. At the later stage, the static yield stress of the paste containing fly ash microbeads is the lowest.

(4) The high solid content and the addition of PCE change the particle packing distribution and hydration reaction rate of UHPC-based pastes, thereby affecting their evolution of static yield stress. At the later stage of the test, the static yield stress of the paste containing fly ash microbeads, slag, ultrafine slag and fly ash increases sequentially compared with that of the blank group. The static yield stress of the paste with 10% of silica fume is higher than that of the blank group, while it is lower when the content of silica fume is 20%.

Author Contributions: Conceptualization, Y.L. and P.Y.; methodology, Y.L.; software, R.J.; validation, Y.L., R.J. and P.Y.; formal analysis, Y.L.; investigation, Y.L.; resources, R.J.; data curation, R.J.; writing—original draft preparation, Y.L.; writing—review and editing, P.Y.; visualization, P.Y.; supervision, P.Y.; project administration, P.Y.; funding acquisition, P.Y. All authors have read and agreed to the published version of the manuscript.

Funding: This research was funded by National Natural Science Foundation of China (No. 51878381).

Institutional Review Board Statement: Not applicable.

Informed Consent Statement: Not applicable.

Data Availability Statement: The data presented in this study are available in the article.

Acknowledgments: The authors would like to acknowledge the National Natural Science Foundation of China (No. 51878381).

Conflicts of Interest: No potential conflict of interest was reported by the authors.

References

1. Costanzi, C.B.; Ahmed, Z.Y.; Schipper, H.R.; Bos, F.P.; Knaack, U.; Wolfs, R.J.M. 3D Printing Concrete on temporary surfaces: The design and fabrication of a concrete shell structure. *Autom. Constr.* **2018**, *94*, 395–404. [CrossRef]
2. Lim, J.H.; Weng, Y.; Pham, Q.-C. 3D printing of curved concrete surfaces using Adaptable Membrane Formwork. *Constr. Build. Mater.* **2020**, *232*, 117075. [CrossRef]
3. Weng, Y.; Li, M.; Ruan, S.; Wong, T.N.; Tan, M.J.; Yeong, K.L.O.; Qian, S. Comparative economic, environmental and productivity assessment of a concrete bathroom unit fabricated through 3D printing and a precast approach. *J. Clean. Prod.* **2020**, *261*, 121245. [CrossRef]
4. Lim, S.; Buswell, R.A.; Le, T.T.; Austin, S.A.; Gibb, A.G.F.; Thorpe, T. Developments in construction-scale additive manufacturing processes. *Autom. Constr.* **2012**, *21*, 262–268. [CrossRef]
5. Zhang, J.; Wang, J.; Dong, S.; Yu, X.; Han, B. A review of the current progress and application of 3D printed concrete. *Compos. Part A Appl. Sci. Manuf.* **2019**, *125*, 105533. [CrossRef]
6. Buswell, R.A.; De Silva, W.R.L.; Jones, S.Z.; Dirrenberger, J. 3D printing using concrete extrusion: A roadmap for research. *Cem. Concr. Res.* **2018**, *112*, 37–49. [CrossRef]
7. Marchment, T.; Sanjayan, J. Mesh reinforcing method for 3D Concrete Printing. *Autom. Constr.* **2020**, *109*, 102992. [CrossRef]
8. Marchment, T.; Sanjayan, J.; Xia, M. Method of enhancing interlayer bond strength in construction scale 3D printing with mortar by effective bond area amplification. *Mater. Des.* **2019**, *169*, 107684. [CrossRef]
9. Lapasin, R.; Longo, V.; Rajgelj, S. Thixotropic Behavior of Cement Pastes. *Cem. Concr. Res.* **1979**, *9*, 309–318. [CrossRef]
10. Khayat, K.H.; Saric-Coric, M.; Liotta, F. Influence of thixotropy on stability characteristics of cement grout and concrete. *Aci Mater. J.* **2002**, *99*, 234–241.
11. Mewis, J.; Wagner, N.J. Thixotropy. *Adv. Colloid Interface Sci.* **2009**, *147–148*, 214–227. [CrossRef]
12. Ferron, R.D.; Shah, S.; Fuente, E.; Negro, C. Aggregation and breakage kinetics of fresh cement paste. *Cem. Concr. Res.* **2013**, *50*, 1–10. [CrossRef]

13. Yim, H.J.; Kim, J.H.; Shah, S.P. Cement particle flocculation and breakage monitoring under Couette flow. *Cem. Concr. Res.* **2013**, *53*, 36–43. [CrossRef]
14. Roussel, N. *Understanding the Rheology of Concrete*; Elsevier: Amsterdam, The Netherlands, 2012.
15. Omran, A.F.; Khayat, K.H. Choice of thixotropic index to evaluate formwork pressure characteristics of self-consolidating concrete. *Cem. Concr. Res.* **2014**, *63*, 89–97. [CrossRef]
16. Omran, A.F.; Naji, S.; Khayat, K.H. Portable Vane Test to Assess Structural Buildup at Rest of Self-Consolidating Concrete. *Aci Mater. J.* **2011**, *108*, 628–637.
17. Roussel, N. Rheological requirements for printable concretes. *Cem. Concr. Res.* **2018**, *112*, 76–85. [CrossRef]
18. Mahaut, F.; Mokéddem, S.; Chateau, X.; Roussel, N.; Ovarlez, G. Effect of coarse particle volume fraction on the yield stress and thixotropy of cementitious materials. *Cem. Concr. Res.* **2008**, *38*, 1276–1285. [CrossRef]
19. Perrot, A.; Lecompte, T.; Khelifi, H.; Brumaud, C.; Hot, J.; Roussel, N. Yield stress and bleeding of fresh cement pastes. *Cem. Concr. Res.* **2012**, *42*, 937–944. [CrossRef]
20. Mahaut, F.; Chateau, X.; Coussot, P.; Ovarlez, G. Yield stress and elastic modulus of suspensions of noncolloidal particles in yield stress fluids. *J. Rheol.* **2008**, *52*, 287–313. [CrossRef]
21. Yuan, Q.; Zhou, D.; Khayat, K.H.; Feys, D.; Shi, C. On the measurement of evolution of structural build-up of cement paste with time by static yield stress test vs. small amplitude oscillatory shear test. *Cem. Concr. Res.* **2017**, *99*, 183–189. [CrossRef]
22. Cheng, D.C.-H.; Evans, F. Phenomenological characterization of the rheological behaviour of inelastic reversible thixotropic and antithixotropic fluids. *Br. J. Appl. Phys.* **1965**, *16*, 1599–1617. [CrossRef]
23. Papo, A. The thixotropic behavior of white Portland cement pastes. *Cem. Concr. Res.* **1988**, *18*, 595–603. [CrossRef]
24. Coussot, P.; Nguyen, Q.D.; Huynh, H.T.; Bonn, D. Viscosity bifurcation in thixotropic, yielding fluids. *J. Rheol.* **2002**, *46*, 573–589. [CrossRef]
25. Roussel, N. A thixotropy model for fresh fluid concretes: Theory, validation and applications. *Cem. Concr. Res.* **2006**, *36*, 1797–1806. [CrossRef]
26. Perrot, A.; Rangeard, D.; Pierre, A. Structural built-up of cement-based materials used for 3D-printing extrusion techniques. *Mater. Struct.* **2016**, *49*, 1213–1220. [CrossRef]
27. Schneider, M.; Romer, M.; Tschudin, M.; Bolio, H. Sustainable cement production—Present and future. *Cem. Concr. Res.* **2011**, *41*, 642–650. [CrossRef]
28. Lothenbach, B.; Scrivener, K.; Hooton, R.D. Supplementary cementitious materials. *Cem. Concr. Res.* **2011**, *41*, 1244–1256. [CrossRef]
29. Juenger, M.C.G.; Siddique, R. Recent advances in understanding the role of supplementary cementitious materials in concrete. *Cem. Concr. Res.* **2015**, *78*, 71–80. [CrossRef]
30. Ahari, R.S.; Erdem, T.K.; Ramyar, K. Thixotropy and structural breakdown properties of self consolidating concrete containing various supplementary cementitious materials. *Cem. Concr. Compos.* **2015**, *59*, 26–37. [CrossRef]
31. Assaad, J.; Khayat, K.H. Assessment of thixotropy of self-consolidating concrete and concrete-equivalent-mortar-effect of binder composition and content. *Aci Mater. J.* **2004**, *101*, 400–408.
32. Yuan, Q.; Zhou, D.; Li, B.; Huang, H.; Shi, C. Effect of mineral admixtures on the structural build-up of cement paste. *Constr. Build. Mater.* **2018**, *160*, 117–126. [CrossRef]
33. Liu, Z.; Li, M.; Weng, Y.; Wong, T.N.; Tan, M.J. Mixture Design Approach to optimize the rheological properties of the material used in 3D cementitious material printing. *Constr. Build. Mater.* **2019**, *198*, 245–255. [CrossRef]
34. Chen, M.; Li, L.; Zheng, Y.; Zhao, P.; Lu, L.; Cheng, X. Rheological and mechanical properties of admixtures modified 3D printing sulphoaluminate cementitious materials. *Constr. Build. Mater.* **2018**, *189*, 601–611. [CrossRef]
35. Chen, M.; Liu, B.; Li, L.; Cao, L.; Huang, Y.; Wang, S.; Zhao, P.; Lu, L.; Cheng, X. Rheological parameters, thixotropy and creep of 3D-printed calcium sulfoaluminate cement composites modified by bentonite. *Compos. Part B Eng.* **2020**, *186*, 107821. [CrossRef]
36. Kawashima, S.; Chaouche, M.; Corr, D.J.; Shah, S.P. Rate of thixotropic rebuilding of cement pastes modified with highly purified attapulgite clays. *Cem. Concr. Res.* **2013**, *53*, 112–118. [CrossRef]
37. Quanji, Z.; Lomboy, G.R.; Wang, K. Influence of nano-sized highly purified magnesium alumino silicate clay on thixotropic behavior of fresh cement pastes. *Constr. Build. Mater.* **2014**, *69*, 295–300. [CrossRef]
38. Panda, B.; Singh, G.V.P.B.; Unluer, C.; Tan, M.J. Synthesis and characterization of one-part geopolymers for extrusion based 3D concrete printing. *J. Clean. Prod.* **2019**, *220*, 610–619. [CrossRef]
39. CEN. *Cement. Part 1: Composition, Specifications and Conformity Criteria for Common Cements*; European Committee for Standardization: Brussels, Belgium, 2011.
40. Ghasemi, Y.; Emborg, M.; Cwirzen, A. Estimation of specific surface area of particles based on size distribution curve. *Mag. Concr. Res.* **2018**, *70*, 533–540. [CrossRef]
41. Ghasemi, Y.; Emborg, M.; Cwirzen, A. Quantification of the Shape of Particles for Calculating Specific Surface Area of Powders. In Proceedings of the International RILEM Conference on Materials, Systems and Structures in Civil Engineering Conference Segment on Simulation Tools Used in the Execution Phase of Concrete Structures, Lyngby, Denmark, 22–24 August 2016.
42. Mostafa, A.M.; Yahia, A. Performance evaluation of different rheometric shearing techniques to disperse concentrated cement suspension. *Appl. Rheol.* **2015**, *25*, 23–31.

43. Kwan, A.K.H.; Fung, W.W.S.; Wong, H.H.C. Water film thickness, flowability and rheology of cement-sand mortar. *Adv. Cem. Res.* **2010**, *22*, 3–14. [CrossRef]
44. Kwan, A.K.H.; Li, L.G. Combined effects of water film thickness and paste film thickness on rheology of mortar. *Mater. Struct.* **2012**, *45*, 1359–1374. [CrossRef]
45. Wong, H.H.C.; Kwan, A.K.H. Packing density of cementitious materials: Part 1—Measurement using a wet packing method. *Mater. Struct.* **2008**, *41*, 689–701. [CrossRef]
46. Kwan, A.K.H.; Wong, H.H.C. Packing density of cementitious materials: Part 2—Packing and flow of OPC plus PFA plus CSF. *Mater. Struct.* **2008**, *41*, 773–784. [CrossRef]
47. Jakob, C.; Jansen, D.; Ukrainczyk, N.; Koenders, E.; Pott, U.; Stephan, D.; Neubauer, J. Relating Ettringite Formation and Rheological Changes during the Initial Cement Hydration: A Comparative Study Applying XRD Analysis, Rheological Measurements and Modeling. *Materials* **2019**, *12*, 2957. [CrossRef]
48. Thomas, J.J.; Biernacki, J.J.; Bullard, J.W.; Bishnoi, S.; Dolado, J.S.; Scherer, G.W.; Luttge, A. Modeling and simulation of cement hydration kinetics and microstructure development. *Cem. Concr. Res.* **2011**, *41*, 1257–1278. [CrossRef]